An Approximate Spectral Clustering Ensemble for High Spatial Resolution Remote-Sensing Images

Kadim Taşdemir, *Member, IEEE*, Yaser Moazzen, and Isa Yildirim

***Abstract*—Unsupervised clustering of high spatial resolution remote-sensing images plays a significant role in detailed land-cover identification, especially for agricultural and environmental monitoring. A recently promising method is approximate spectral clustering (SC) which enables spectral partitioning for large datasets to extract clusters with distinct characteristics without a parametric model. It also facilitates the use of various information types via advanced similarity criteria. However, it requires an empirical selection of a similarity criterion optimal for the corresponding application. To address this challenge, we propose an approximate SC ensemble (ASCE2) which fuses partitionings obtained by different similarity representations. Contrary to existing spectral ensembles for remote-sensing applications, the proposed ASCE2 employs neural gas quantization instead of random sampling, advanced similarity criteria instead of traditional distance-based Gaussian kernel with different decay parameters, and a two-level ensemble. We evaluate the proposed ASCE2 with three measures (accuracy, adjusted Rand index, and normalized mutual information) using five remote-sensing images, two of which are commonly available. We apply the ASCE2 in two applications for agricultural monitoring: 1) land-cover identification to determine orchard fields using a WorldView-2 image (0.5-m spatial resolution) and 2) finding lands in good agricultural condition using multitemporal RapidEye images (5-m spatial resolution). Experimental results indicate a significant betterment of the resulting partitionings obtained by the proposed ensemble, with respect to the evaluation measures in these applications.**

***Index Terms*—Approximate spectral clustering (SC), cluster ensemble, clustering, geodesic similarity, land-cover identification.**

I. Introduction

THE SPATIAL resolution of remote-sensing images has become below meter resolution with increased number of spectral bands. This increased (very) high spatial resolution enables detailed spectral, textural, or structural representation to extract accurate information in a supervised or unsupervised manner for agricultural and environmental control, urban monitoring, disaster management, and homeland security (see [1]–[3] and references therein). Supervised approaches require heavy expert time and labeled training points (which are often hard and expensive to get since they can be purely obtained only with *in situ* measurements [4]). It becomes more challenging for agricultural monitoring where crop calendar, seasonal, and regional changes play a significant role in spectral signatures of the land cover/use classes [5], [6]. Therefore, achieving supervised classification performances with unsupervised approaches (which need no labeled points and only limited expert interaction) is of great importance for effective agricultural control at the state level.

Traditional unsupervised k-means and its variant ISODATA methods are usually poor in performance due to being centroid-based parametric models which produce (hyper-) spherical clusters [5], [7]. Alternative approaches without centroid models (hierarchical clustering [8], neural clustering [9], spectral clustering (SC) [10]–[12] to name a few) are shown more successful than k-means for remote-sensing images, thanks to their relatively accurate representation of true clusters. Among them, SC, which has the ability to extract clusters of different characteristics without a parametric model, has been recently popular [10]–[13]. Due to its computational complexity, SC is performed for high spatial resolution remote-sensing images through a two-step approach called approximate SC (ASC), i.e., the SC is applied to the data representatives selected by sampling or quantization [10], [12]–[16]. The ASC enables the advantages of SC for large remote-sensing images and integrates different information types (such as distance, density, and topology) to produce an effective information representation for extraction of precise cluster structure [17]. However, it necessitates an optimum selection for similarity definition tailored to the application requirements. Instead of empirical determination of optimal conditions, the partitionings obtained with different settings can be fused by ensemble learning.

The ensemble methods merge the partitionings obtained by different input or feature sets, distinct methods, or the same method with several parameter settings, using various approaches such as majority voting, evidence accumulation, hyper graph operations, metaclustering, or mixture models [10], [18]–[23]. When they are used to fuse the decisions of the same method with several parameter settings, as in SC ensembles (SCE) [10], [22], [23], they eliminate the need to determine the optimal parameter values. For example, the SCE in [10], which uses random sampling (Nystrom method [14]) together with maximum voting and metaclustering algorithm, combines partitionings obtained with different kernel parameter values in similarity definition, for segmentation of relatively small SAR images [10]. A similar approach is also used for image

Manuscript received September 27, 2014; revised March 15, 2015; accepted April 14, 2015. Date of publication May 06, 2015; date of current version July 20, 2015. This work was supported by TUBITAK Career under Grant 112E195. The work of author K. Taşdemir is also supported by EU FP7 Marie Curie Career Integration under Grant IAM4MARS. *(Corresponding author: Kadim Taşdemir.)*

K. Taşdemir is with the Department of Computer Engineering, Antalya International University, Antalya 07190, Turkey (e-mail: kadim.tasdemir@antalya.edu.tr).

Y. Moazzen is with Istanbul Technical University, Istanbul 34469, Turkey.

I. Yildirim is with Istanbul Technical University, Istanbul 34469, Turkey, also with Abdullah Gul University, Kayseri 38080, Turkey, and also with the University of Illinois, Chicago IL 60607 USA.

Color versions of one or more of the figures in this paper are available online at http://ieeexplore.ieee.org.

Digital Object Identifier 10.1109/JSTARS.2015.2424292

1939-1404 © 2015 IEEE. Personal use is permitted, but republication/redistribution requires IEEE permission.
See http://www.ieee.org/publications_standards/publications/rights/index.html for more information.

Authorized licensed use limited to: Abdullah GUl Univ (KAYSERI ABDULLAH GUL UNIVERSITESI). Downloaded on March 31,2023 at 06:40:09 UTC from IEEE Xplore. Restrictions apply.

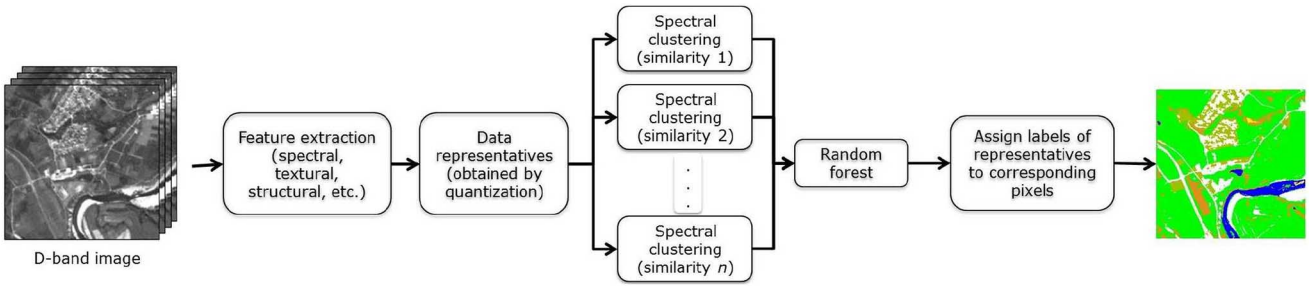

Fig. 1. ASC ensemble (ASCE). Spectral or spatial features relevant to remote-sensing application are extracted (beyond the scope of this paper). The N_r data representatives are selected by neural gas quantization of these features. The data representatives are partitioned by SC using n_s similarity criteria in Section II-C with n_{km} k-means runs. The resulting partitions are merged with cluster ensemble as explained in Section II-D. The ensemble labels of the representatives are assigned to their corresponding data points (pixels).

segmentation [22]. Despite the ensemble approach, different parameter windows, specific to the datasets, are used to achieve high performance [10]. In addition, when random sampling is used for SC of large datasets, out-of-sample labeling may become problematic [16], [24].

In this paper, we propose an ASC ensemble (ASCE2) for unsupervised clustering of large remote-sensing images. The ASCE2 is novel in three ways. First, we obtain the data representatives using neural gas [25] (instead of Nystrom approximation), to get smaller quantization errors and address out-of-sample labeling problem. Second, we use the recent similarity definitions [13], [17] exploiting various information types, rather than the traditional distance-based Gauss kernel with different parameter values. Third, we have a two-level ensemble method which obtains a fused decision for each similarity criterion and then merges these decisions into a consensus label. We test the ASCE2 performance on two commonly available remote-sensing data (Statlog [26] and Boston [27]) and three remote-sensing images for agricultural control. Based on the evaluation by accuracies, adjusted Rand index (ARI) and normalized mutual information (NMI), we show that the proposed ASCE2 achieves high performance with respect to all three evaluation measures. The rest of the paper is outlined as follows. We first introduce the proposed ASCE2 step by step in Section II. We then discuss the experimental results in Section III and conclude in Section IV.

II. ASC Ensemble

The proposed ASCE2 merges the partitionings obtained by ASC with different similarity criteria. It has two parts: ASC and ensemble learning. ASC applies SC on a reduced set of data representatives selected by sampling or quantization [12], [14]–[16] so that it enables the use of SC in remote-sensing images to extract clusters of distinct characteristics without a parametric model. Sampling-based ASCs are faster than quantization-based ASCs in expense of a lower clustering performance due to relatively high quantization errors and out-of-sample labeling challenge [12], [16], [24]. The neural gas quantization [25] is shown more successful than k-means and its variants for ASC in remote-sensing image analysis [12], [13]. After selecting representatives, ASC is similar to the SC approaches. Yet, the use of representatives in ASC enables manifold-based similarity definitions (such as data topology and local density) in addition to the traditional distance-based similarities [13], which produces distinct partitionings. Ensemble learning combines the resulting partitionings to have a consensus on the label of data representatives. Then, the label of each representative is assigned to its corresponding image pixels. An outline of the ASCE2 method is shown in Fig. 1 and summarized in Table I. We now briefly explain the ASCE2.

TABLE I
APPROXIMATE SPECTRAL CLUSTERING ENSEMBLE

1. *Approximate spectral clustering*
   Input: Selected features of the remote sensing image
   Obtain N_r representatives by neural gas quantization
   Apply spectral clustering to N_r representatives using n_s similarities in Section II-C with n_{km} k-means runs
   Output: $n_s n_{km}$ partitionings of N_r representatives
2a. *Cluster ensemble — Alternative 1 (ASCE1)*
   Input: $n_s n_{km}$ partitionings of the N_r representatives
   Construct a similarity matrix S_{CE1} by the identically labelled representatives among all partitionings (12)
   Apply spectral clustering based on S_{CE1}
   Output: Final partitioning of N_r representatives
2b. *Cluster ensemble — Alternative 2 (2-step) (ASCE2)*
   Input: $n_s n_{km}$ partitionings of the N_r representatives
   Obtain a similarity matrix S_{CE2a} using the number of identically labelled representatives among n_{km} different partitionings of each similarity criterion
   Apply spectral clustering based on these S_{CE2a} to obtain n_s first level ensemble partitionings
   Obtain a similarity matrix S_{CE2b} using the number of identically labelled representatives among the resulting n_s ensemble partitionings
   Apply spectral clustering based on S_{CE2b}.
   Output: Final partitioning of N_r representatives
3. *Assign the representatives' labels to their corresponding pixels.*

A. Data Representatives by Neural Gas Quantization

As a first step in ASCE2, we obtain data representatives by neural gas quantization [25]. Being a neural learning paradigm, the neural gas [25] quantizes the data points in a topology preserving manner based on neighborhood ranking. Its randomly initialized neural units evolve to the quantization representatives with an iterative learning: a data point v is randomly selected from the dataset at each step, and its best-matching unit (BMU) w_i is found by the minimum distance

$$||v - w_i|| \leq ||v - w_j||. \quad (1)$$

Authorized licensed use limited to: Abdullah GUl Univ (KAYSERI ABDULLAH GUL UNIVERSITESI). Downloaded on March 31,2023 at 06:40:09 UTC from IEEE Xplore. Restrictions apply.

Then, the neural units w_j neighbor to the BMU w_i are determined by a neighborhood function $h_\tau(w_j) = \exp(-\rho_{w_i}/\tau)$ based on ρ_{w_j} which is the rank of the distance of w_j to v. Note that the rank $\rho_{w_i} = 0$. Finally, w_i and its neighbors w_j are adapted by

$$w_j(t+1) = w_j(t) + \alpha(t)h_\tau(w_j)(v - w_j(t)) \tag{2}$$

where $\alpha(t)$ is a learning parameter decaying by time. When this iterative process is completed by a predetermined stop criterion, the neural units become the quantization representatives, achieving a lower quantization error than k-means [25].

B. SC of Data Representatives

SC methods are manifold learning approaches, which successfully extract clusters with different characteristics, thanks to their nonparametric model approach and easy implementation [28]–[30]. They are based on eigendecompositon of a graph Laplacian derived from pairwise similarities of the data points. This results in heavy computational load, which makes them inapplicable for large datasets such as remote-sensing images with high spatial resolution. To exploit SC advantages for these datasets, ASC performs SC on a reduced set of data representatives.

Being associated with relaxed optimization of graph-cut problems, SC constructs a graph *Laplacian* matrix L based on some optimization criteria [28]–[30]. Due to the fact that there is no clear advantage among SC methods as long as a normalized graph Laplacian is used [31], [32], we employ the SC method in [29] to cluster the data representatives obtained by neural gas: Let $G = (V, S)$ be a weighted undirected graph where its nodes V represent the representatives and the edges S are the pairwise similarities between them. The normalized Laplacian matrix L_{norm} is defined as

$$L_{norm} = D^{-1/2} S D^{-1/2} \tag{3}$$

based on a similarity matrix S and its diagonal degree matrix D with $d_i = \sum_j s(i,j)$. Then, the SC method is as follows.

1) Construct a similarity matrix S showing the pairwise similarities of the N_r representatives to be clustered;
2) Calculate D and L_{norm} using the similarity matrix S;
3) Find the k eigenvectors $\{e_1, e_2, \ldots, e_k\}$ of L_{norm}, associated with the k highest eigenvalues $\{\lambda_1, \lambda_2, \ldots, \lambda_k\}$;
4) Construct the $N_r \times k$ matrix $E = [e_1 e_2 \ldots e_k]$ and obtain $N_r \times k$ matrix U by normalizing the rows of E to have norm 1, i.e., $u_{ij} = \frac{e_{ij}}{\sqrt{\sum_k e_{ik}^2}}$;
5) Cluster the N_r rows of U with k-means into k clusters.

The eigendecomposition of the graph Laplacian (ideally) produces a data projection where submanifolds (clusters) are well separated. A simple method in Step 5, such as k-means, is hence expected to produce a clear delineation among clusters. However, this is often not possible due to complex data structures, resulting in intersecting submanifolds. Therefore, consecutive k-means runs may result in distinct partitionings, due to the randomness in k-means algorithm [13].

C. Similarity Criteria for ASC

The similarity criterion to be set for S plays a significant role to achieve an accurate cluster extraction. The pairwise similarities in SC $s(i,j)$s are traditionally determined by a Gaussian kernel based on the (Euclidean) distances $d_{Euc}(x_i, x_j)$, with a global decaying parameter σ (to be optimally found through experiments [29] or a local σ_i reflecting the distance to the kth-nearest neighbor of x_i [33])

$$s_{Euc}(i,j) = \exp\left(-\frac{d_{Euc}(x_i, x_j)}{2\sigma_i \sigma_j}\right). \tag{4}$$

However, for ASC, new information types such as topology, density can be embedded into S for more effective definition for pairwise similarities of the data representatives [12], [17], [34]. A recent approach [12] uses a similarity measure (CONN) that exploits local density together with data topology on the representative level. $CONN(i,j)$ shows the number of data points for which the representatives w_i and w_j are the pair of the best-matching and the second-BMUs. In other words, $CONN(i,j)$ represents the local density distribution inside the subregions $V_{ij} \cup V_{ji}$ of the Voronoi polygons V_i and V_j, (V_i is the set of data points v for which w_i is the closest representative), i.e.,

$$CONN(i,j) = |V_{ij} \cup V_{ji}| \tag{5}$$

where the sub-Voronoi polyhedron V_{ij} is

$$V_{ij} = \{v \in V_i : ||v - w_j|| \leq ||v - w_k|| \; \forall k \neq i\}. \tag{6}$$

By its definition, CONN is a weighted version of the induced Delaunay triangulation in [25] showing the neighbors according to the manifold, where weights indicate how the data points are distributed within the Voronoi polygons. CONN thus produces more accurate partitionings than those obtained by distance-based approaches [12], [35]. The distance information is also integrated with CONN for ASC by a hybrid similarity criterion S_{hyb} [34] where

$$s_{hyb}(i,j) = s_{Euc}(i,j) \times \exp\left(\frac{CONN(i,j)}{\max_{i,j} CONN(i,j)}\right). \tag{7}$$

The hybrid S_{hyb} actually scales the distance-based similarity with respect to local density distribution and data topology. If $CONN(i,j) = 0$, then two representatives w_i and w_j are not neighbors, which results in $s_{hyb}(i,j) = s_{Euc}(i,j)$. Otherwise, their similarity is scaled by $[1, e]$, producing a greater similarity upto a scale of e for the maximum $CONN(i,j)$.

Recently, geodesic-based approaches are also proposed for ASC [13], [17]. To calculate geodesic distances, a preliminary step is to determine a neighborhood graph showing the neighbor representatives in the manifold. A traditional way to construct this graph is the use of (mutual) k-nearest neighbor ($k - nn$) graph. If w_i and w_j are among their k-closest neighbors, they are neighbors. Then, the geodesic distance between w_i and w_j is the sum of Euclidean distances of their shortest path

$$d_{geoknn}(w_i, w_j) = \sum_{lm \in SP_{knn}(w_i, w_j)} d_{Euc}(l,m) \tag{8}$$

Authorized licensed use limited to: Abdullah GUl Univ (KAYSERI ABDULLAH GUL UNIVERSITESI). Downloaded on March 31,2023 at 06:40:09 UTC from IEEE Xplore. Restrictions apply.

where $SP_{knn}(w_i, w_j)$ is the set of edges in the shortest path between w_i and w_j calculated with d_{Euc} and $k-nn$ graph. The parameter k should be optimally set; however, k may be different for each representative. As a topology-based alternative reflecting local characteristics, CONN can be used for neighborhood graph in calculating geodesic distances to find specific number of neighbors for each representative [17]. The geodesic distance d_{geoadj} based on CONN graph using Euclidean distances d_{Euc} is calculated as

$$d_{geoadj}(w_i, w_j) = \sum_{lm \in SP_{adj}(w_i, w_j)} d_{Euc}(l, m) \tag{9}$$

where $SP_{adj}(w_i, w_j)$ is the set of edges in the shortest path between w_i and w_j based on d_{Euc} and CONN neighborhood graph. Instead of distances, local density distribution can also be used for geodesic distance calculation. Namely, using density-based distance

$$d_{CONN}(w_i, w_j) = \begin{cases} e^{-\frac{CONN(i,j)}{\max_{y,z} CONN(y,z)}}, & \text{if } CONN(i,j) > 0 \\ \infty, & \text{otherwise} \end{cases}$$

a geodesic distance including both data topology and the data distribution can be defined as [17]

$$d_{geoconn}(w_i, w_j) = \sum_{lm \in SP_{conn}(w_i, w_j)} d_{CONN}(l, m). \tag{10}$$

$SP_{conn}(w_i, w_j)$ is now the set of edges in the shortest path between w_i and w_j with respect to d_{CONN} distance and CONN neighborhood. In addition, to exploit all available information for ASC on the representative level, a hybrid approach $d_{geohyb}(w_i, w_j)$ merging both distance and density using CONN graph can be defined as

$$d_{geohyb}(w_i, w_j) = \sum_{lm \in SP_{hyb}(w_i, w_j)} d_{Euc}(l, m) d_{CONN}(l, m). \tag{11}$$

The geodesic distance-based similarities are then obtained by replacing d_{Euc} in (4) with the corresponding distance criterion. They achieve better clustering accuracies for a wide variety of datasets with different clustering statistics [13]. Despite their success, they may not achieve the best partitioning for each dataset. Therefore, instead of finding a best criterion for various applications, fusing the partitionings obtained by different criteria with ensemble approach will exploit different properties to reach a consensus in clustering.

D. Cluster Ensemble

In order to achieve better performances with ensembles than with single partitionings, it is important to have diverse results obtained by different feature sets, subsets, clustering methods, or different parameters for the same method. In our approach, we produce a set of (neural gas) data representatives and obtain diversity with various similarity criteria (measuring distance, topology, and density) and random initializations for k-means step in SC. By the use of data representatives, graph-based ensemble approach [18]—which is infeasible for large data—can be easily applicable for an effective decision fusion. A graph $G = (V, S_{CE})$ is constructed based on $n_s \times n_{km}$ partitionings obtained by n_s similarity criteria and n_{km} k-means runs per similarity criterion, where $S_{CE}(i, j)$ shows the pairwise similarity of the representatives w_i and w_j with respect to the number of partitionings for which they have the same label, i.e.,

$$S_{CE}(i, j) = \sum_{m=1}^{n_s} \sum_{k=1}^{n_{km}} S_{m,k}(i, j) \tag{12}$$

where $S_{m,k}(i, j) = 1$ if w_i and w_j are in the same cluster; otherwise, $S_{m,k}(i, j) = 0$. An SC is applied to this graph to get the consensus labels for the representatives. We call this one-level ensemble as ASCE1.

Alternative to the traditional approach of fusing all results into one as in ASCE1, we use a two-level ensemble process (ASCE2). In ASCE2, we first get an ensemble for a similarity criterion s_* from its corresponding partitionings obtained by n_{km} k-means runs, based on a similarity matrix $S_{CE2a} = \sum_{k=1}^{n_{km}} S_{s_*,k}$. We then fuse n_s ensemble results of each similarity (Section II-C) using $S_{CE2b} = \sum_{m=1}^{n_s} S_m$. By its construction, the two-level ASCE2 first addresses the randomness in k-means and then exploits distinct results obtained by different information types. Note that we fuse the clustering labels at the representative level and then determine the labels of the data points according to the ensemble labels of their representatives. Table I outlines the proposed ASCE.

III. Experimental Results

We evaluate the performance of the proposed ASCE2 performance based on accuracy (percentage of correctly labeled data), ARI [36], and NMI [37] using five remote-sensing image datasets (Statlog [26], Boston [27], Bengisu [38], [39], KARD and VARN [6]). Two datasets (Statlog and Boston) are commonly available, whereas the last three are obtained for agriculture monitoring.

A. Datasets

The Statlog dataset is available from UCI Machine Learning Repository [26]. It is a relatively small dataset composed of 6435 points with four features representing spectral values. There are six classes: red soil, cotton crop, gray soil, damp gray soil, soil with vegetation stubble, and very damp gray soil. The Boston dataset [27] is obtained from a Landsat 7 Thematic Mapper satellite (available: http://techlab.bu.edu/resources/data/C50). It is a remote-sensing image of 360×600 pixels, where each pixel has 41 features reflecting spectral and textural characteristics. Fig. 2 shows an RGB color composite of the Boston dataset which has eight classes: beach, ocean, ice, river, road, park, residential, and industrial. 29 003 pixels are labeled to these eight classes to represent the ground truth [27].

Authorized licensed use limited to: Abdullah GUl Univ (KAYSERI ABDULLAH GUL UNIVERSITESI). Downloaded on March 31,2023 at 06:40:09 UTC from IEEE Xplore. Restrictions apply.

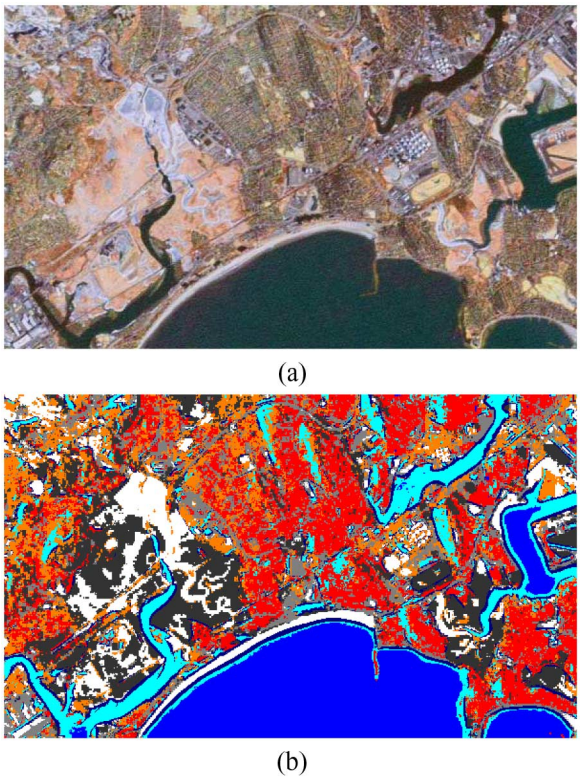

Fig. 2. Boston remote-sensing dataset. (a) Natural color composite of the dataset (316×600 pixels). (b) Resulting clustermap obtained by ASCE2. Each color indicates one of the eight extracted clusters.

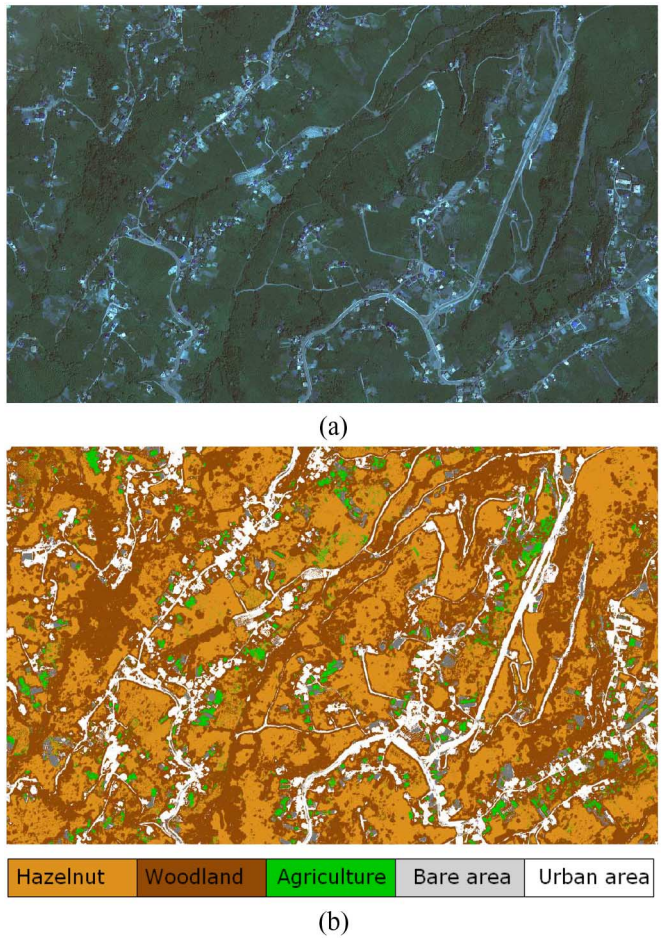

Fig. 3. Bengisu dataset for hazelnut detection (2918×4775 pixels). (a) Natural color composite using red, green, and blue spectral bands of the Worldview2 image. The hazelnut orchards are the main land cover of the region. (b) ASCE2 cluster map with five land cover types.

As a very high spatial resolution example, we use a WorldView-2 image (0.5-m spatial resolution) for land-cover identification to extract hazelnut fields. The eight-band multispectral and panchromatic WorldView-2 images were provided through WorldView-2 eight-band challenge organized in 2010. The (2918×4775-pixel) image covers an approximately $3.5\,\mathrm{km}^2$ region (Bengisu, Trabzon) on the Black Sea coast of Turkey, where hazelnut is the main agricultural crop together with few other classes which are grouped into woodlands (deciduous and coniferous forests, other orchards as well as hedges), other agricultural lands (vegetated areas except hazel orchards and woodlands), bare soil and nonagricultural areas (urban, commercial, and industrial areas, roads, water bodies) [38], [39]. Fig. 3 provides a natural color composite of the image. A total of 222 437 test pixels (90 072 woodlands, 82 824 hazelnut, 14 488 urban, 18 442 agriculture, and 16 611 bare area) were randomly determined proportional to their land coverage in the study area, using field study and domain knowledge of the national experts [39]. Referring to [38] and [39] for details of the study area and existing challenges in extraction of hazelnut fields in this region, supervised classification accuracies for five classes were 76.4% for eight multispectral bands and 83.2% for fused features (eight multispectral and four Gabor features). We therefore use fused features to evaluate the proposed ASCE2.

The KARD and VARN datasets are multitemporal RapidEye images (5-m spatial resolution), used in [6] and [8], for land-cover identification in Bulgaria to determine land parcels in good agricultural condition (GAC) that are potentially applicable for payments in the frame of the Common Agricultural Policy of the European Union. This GAC analysis requires extraction of four classes: water, permanent bare areas (including artificial sealed surfaces), forest, and vegetated areas. Each image is a subset of stacked multitemporal data obtained by 5-band RapidEye images acquired in 4 consecutive months from April to July 2009. This produces 20-band images, resulting in 20-D spectral features. The KARD image (with 4 million pixels) is a zone in Kardjali (an area in the southeast of Bulgaria), whereas VARN (with approximately 8 million) is a region from Varna (an area in the east of Bulgaria). Their natural color composites are shown in Fig. 4 to reflect their landscapes. The KARD zone is a complex landscape from a highly segmented section of Strumni Ridge in the area of Eastern Rhodope. It has a hilly-to-mountainous relief with deforested and eroded slopes. Deciduous forest covers the mountain ridges and upper hills, while patches of coniferous forests are presented in lower altitudes along with bare areas with sparse vegetation. There is a river, crossing the area from south to north (left of the image), with a sandy and rocky riverbed. Main urban structures are mainly around the river

Authorized licensed use limited to: Abdullah GUl Univ (KAYSERI ABDULLAH GUL UNIVERSITESI). Downloaded on March 31,2023 at 06:40:09 UTC from IEEE Xplore. Restrictions apply.

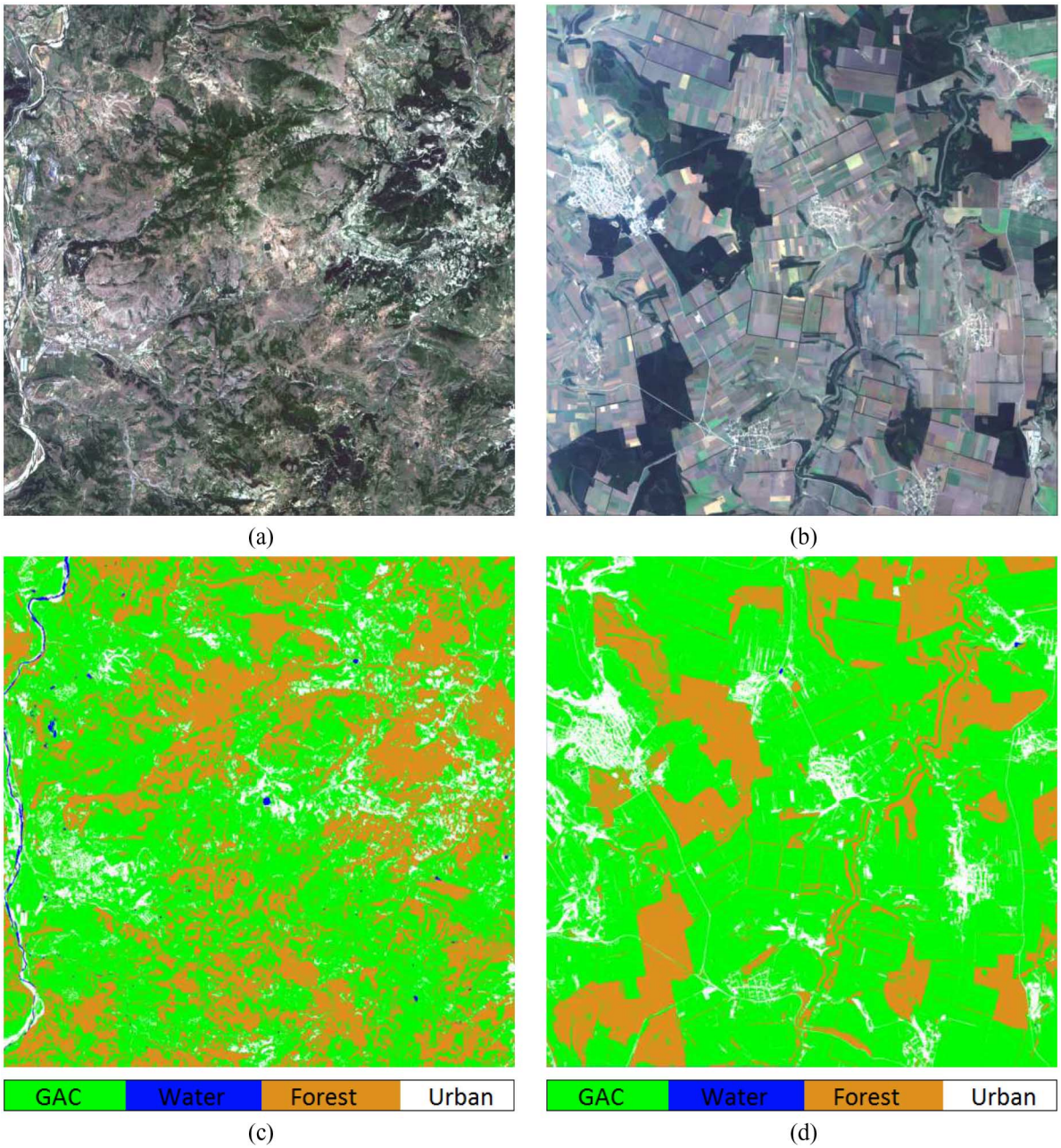

Fig. 4. Multitemporal RapidEye images and their ASCE results. First row shows natural color composites of the images acquired in June 2009 for evaluation of the land cover. (a) KARD. (b) VARN. (Details on these regions can be found in [6].) The second row shows clustering maps. (c) KARD. (d) VARN.

together with small villages across the scene. There are also some small dams and ponds close to the urban areas, used for water supply and irrigation. Contrary to the KARD zone, VARN represents a highly productive region where the agricultural fields can easily be identified from its color composite. In addition, dark areas indicate forested regions, whereas white color shows mainly urban structures. We refer to [6] for more details on these datasets.

B. Performance Evaluation

We use three measures to evaluate the partitionings of these remote-sensing images: accuracy, ARI, and NMI. Accuracy is the percentage of correctly clustered data points. ARI [36] is a measure of agreement between labels obtained by a clustering process and the other labels defined by external criteria for the same data [40]. ARI considers not only the correct separation of data points into different clusters but also the relation between data points of the same cluster, to sensitively evaluate the relation between each datum and its target label for multiclass problems [40]. NMI is used to compare the resulting partitionings in an information theoretical way [37].

We first get 1600 representatives for each dataset (except Statlog for which 644 representatives are obtained due to its relatively small size) by neural gas using SOMtoolbox (available: http://www.cis.hut.fi/somtoolbox/) with default parameters.

Authorized licensed use limited to: Abdullah GUl Univ (KAYSERI ABDULLAH GUL UNIVERSITESI). Downloaded on March 31,2023 at 06:40:09 UTC from IEEE Xplore. Restrictions apply.

TABLE II
ACCURACIES OF ASCE FOR FIVE REMOTE-SENSING IMAGE DATASETS

Similarity criterion	Statlog		Boston		Bengisu		KARD		VARN	
	Average	ASCE	Average	ASCE	Average	ASCE	Average	ASCE	Average	ASCE
s_{Euc}	66.90 (3.3)	69.03	91.04 (1.2)	91.93	62.37	68.03	83.85 (2.6)	92.25	93.07 (1.1)	93.28
s_{CONN}	57.84 (14.9)	56.83	82.34 (4.7)	83.31	74.49	75.70	94.24 (0.8)	95.19	93.35 (0.3)	93.80
s_{hyb}	49.31 (10.6)	48.31	85.42 (2.5)	85.52	72.76	73.05	82.98 (2.6)	85.56	93.12 (0.8)	92.76
s_{geoknn}	65.77 (5.0)	67.15	89.69 (2.6)	91.42	50.02	61.38	66.34 (0.6)	69.25	82.83 (5.3)	92.76
s_{geoadj}	63.40 (5.8)	65.35	96.27 (0.9)	96.51	73.05	73.88	88.96 (3.1)	93.85	87.91 (1.4)	90.96
$s_{geoconn}$	54.61 (4.8)	54.61	94.06 (1.5)	94.52	75.83	74.73	92.14 (1.2)	91.71	89.02 (1.4)	89.66
s_{geohyb}	63.71 (6.2)	63.71	96.08 (0.9)	96.30	74.27	**77.13**	94.88 (1.3)	95.19	92.40 (2.1)	90.18
ASCE1		63.14		96.69		75.24		**95.45**		93.33
ASCE2		**69.23**		**96.70**		75.47		**95.45**		**94.68**

TABLE III
ARI VALUES FOR THREE REMOTE-SENSING IMAGES

Similarity criterion	Bengisu		KARD		VARN	
	Mean	ASCE	Mean	ASCE	Mean	ASCE
s_{Euc}	0.28	0.32	0.695	0.811	0.816	0.837
s_{CONN}	0.39	0.41	0.864	0.853	0.818	0.830
s_{hyb}	0.37	0.37	0.687	0.705	0.813	0.797
s_{geoknn}	0.14	0.23	0.315	0.323	0.568	0.779
s_{geoadj}	0.38	0.39	0.818	0.895	0.688	0.710
$s_{geoconn}$	0.42	0.41	0.846	0.886	0.726	0.720
s_{geohyb}	0.41	**0.45**	0.897	0.907	0.813	0.840
ASCE1		0.41		0.900		0.840
ASCE2		0.41		**0.910**		**0.870**

TABLE IV
NMI VALUES FOR THREE REMOTE-SENSING IMAGES

Similarity criterion	Bengisu		KARD		VARN	
	Mean	ASCE	Mean	ASCE	Mean	ASCE
s_{Euc}	0.44	0.46	0.696	0.806	0.765	0.789
s_{CONN}	0.52	**0.54**	0.831	0.858	0.781	0.787
s_{hyb}	0.50	0.50	0.673	0.695	0.764	0.748
s_{geoknn}	0.30	0.37	0.396	0.369	0.600	0.690
s_{geoadj}	0.49	0.50	0.766	0.863	0.656	0.671
$s_{geoconn}$	0.52	0.51	0.796	0.831	0.656	0.608
s_{geohyb}	0.50	**0.54**	0.867	**0.879**	0.757	0.796
ASCE1		0.53		0.860		0.770
ASCE2		**0.54**		0.870		**0.810**

The ratios of the number of representatives to the number of data points are 10% for Statlog, 6.25% for Boston, 0.04% for KARD, 0.02% for VARN, and 0.01% for Bengisu. Based on these representatives, we extract 20 partitionings for each similarity criterion (due to random initialization in k-means step at the SC). Table II shows the clustering accuracies averaged over 20 runs for five datasets. (We note that different numbers of k-means runs are also tested, producing insignificant changes in performance.) Additionally, Tables III and IV provide average ARI and NMI values, respectively. Then, we get the two-level ASCE2 ensemble labels: 1) a cluster ensemble is run for corresponding similarity to fuse different partitionings obtained by random initialization of k-means step in SC and 2) the fused partitionings of each similarity are merged to produce the final labels.

The best performance for single approximate clustering method is obtained by the recently proposed geodesic based similarity criteria for four datasets (except Statlog), which in turn shows their power in delineating cluster boundaries with respect to different information types. In addition, the first-level ensemble already improves the performance for all five datasets. Of 35 cases (7 similarity and 5 datasets), there are only 5 exceptions for accuracy: s_{CONN} and s_{hyb} for Statlog, $s_{geoconn}$ for KARD (0.4% decrease), and hybrid criteria s_{hyb} and s_{geohyb} for VARN. Similarly, there is only one exception for KARD (s_{CONN}) and one for VARN (s_{hyb}) with respect to ARI values, and there are only three exceptions with respect to NMI values. For the rest, the performance improvement is usually significant in all three measures, i.e., upto 11% increase in accuracy (for s_{geoknn}), upto 0.21 increase in ARI (for s_{geoknn}), and 0.09 increase in NMI. The accuracy of 77.13% for Bengisu is greater than classification accuracy of 76.4% obtained by spectral features in [39] and close to their classification accuracy of 83.2% with the same merged features. Achieving accuracies similar to the ones obtained by supervised approaches show the effective information representation ability of the recent geodesic similarity combined with the ensemble.

An interesting point is that the ensemble of k-means runs may change the performance ranking of the similarity criteria, i.e., the most suitable similarity for the application. For example, $s_{geoconn}$ has the greatest accuracy of 75.83% for Bengisu, whereas s_{geohyb} has a greater accuracy of 77.13% after ensemble. Similarly, $s_{geoconn}$ has the greatest ARI value 0.42 and NMI value 0.52 for Bengisu, whereas s_{geohyb} has greater values (0.45 and 0.54, respectively) after ensemble. These results conclude that an ensemble can achieve higher accuracies than single run, even though only diversity between these runs is random initialization of k-means step in the algorithm. Ensemble of these results using ASCE1 and ASCE2 will reduce the necessity to select the best similarity for a given application while aiming to achieve a better partitioning.

The proposed two-level ensemble ASCE2 achieves the best performance for four datasets in terms of accuracy (except Bengisu). The improvement in accuracy is significant for these datasets: 2.3% increase for Statlog (from the best average of s_{Euc} 66.9% to 69.2%); a 0.4% increase for Boston (from the best average of s_{geoadj} 96.3% to 96.7%); 0.6% increase for KARD (from the best average of s_{geohyb} 94.9% to 95.5%);

Authorized licensed use limited to: Abdullah GUl Univ (KAYSERI ABDULLAH GUL UNIVERSITESI). Downloaded on March 31,2023 at 06:40:09 UTC from IEEE Xplore. Restrictions apply.

1.3% increase for VARN (from 93.4% with s_{CONN} to 94.7%). For Bengisu, however, there is a decrease in accuracy. The ensemble accuracy of 75.5% is close to the best result with a single clustering (75.8% with $s_{geoconn}$) and significantly greater than the second best result (74.5% with s_{CONN}). Similarly, according to ARI values, the ASCE2 produces a 0.01 increase for KARD and 0.05 increase for VARN. For NMI evaluation, the ASCE2 has an improvement of 0.02 for Bengisu, and of 0.03 for VARN. Figs. 2–4 show the resulting cluster maps for the Boston, Bengisu, KARD, and VARN datasets, respectively. The visual comparison of these cluster maps with the natural color composites indicates a striking fit of the extracted clusters. These analyses indicate that the consensus labelings achieved by the proposed ensemble are in line with the natural clusters in terms of desired classes and information theoretical way.

To compare the ASCE2 performance with the traditional ensemble approaches, we fuse all 140 partitionings (7 criteria and their corresponding 20 runs) with ASCE1 at once. We obtain an accuracy of 63.14% for Statlog, 96.69% for Boston, 75.24% for Bengisu, 95.45% for KARD, and 93.33% for VARN. These accuracies are smaller than a single clustering method for three datasets (Statlog, Bengisu, and VARN). However, the ASCE1 ensemble has a better ARI value than any single clustering for KARD and VARN, and a very close value for Bengisu. The ASCE1 ensemble has also a better NMI value than any single clustering for Bengisu and smaller NMI values by a close margin for KARD and VARN. The two-level ASCE2 is significantly better than the ASCE1 with traditional one-level ensemble: ASCE2 achieves greater accuracies for four datasets, except KARD for which their accuracies are equal (Table II), greater ARI values for two of the three datasets (Table III), and greater NMI values for three datasets (Table IV). The proposed ASCE2 can hence be a powerful tool for unsupervised cluster extraction in remote-sensing applications.

IV. Conclusion

High spatial resolution has brought new challenges for remote-sensing image analysis while creating emerging applications due to improved abilities of fine details for precise agriculture, homeland security, and urban monitoring. A long-standing challenge for remote-sensing images, and for those with high spatial resolution, is the necessity of accurate labeled training sets (which can only be obtained purely from the field visits) to achieve effective land-cover maps with many supervised approaches [41]. While active learning approaches [42] address this by reducing the required labeled samples and guiding the user to label few selected samples, unsupervised clustering uses no labeled samples. Recently, ASC methods enable the spectral partitioning of large datasets such as remote-sensing images with high spatial resolution, to utilize its advantages of extracting clusters with various characteristics without a parametric model. The ASC methods also enable effective manifold-based information representation criteria that are optimally selected for corresponding application. To harness different information types in ASC without a need for optimality selection, we introduced an ASCE2 composed of three stages: 1) neural gas quantization to obtain data representatives; 2) SC of these representatives with recent similarity criteria derived from different information types exploiting distinct manifold characteristics; and 3) a two-level graph-based ensemble of obtained partitionings. We showed that the ASCE2 improves the clustering quality with respect to three measures (accuracy, ARI, and NMI) for five remote-sensing images. Based on its success on remote-sensing applications for land-cover identification, the ASCE2 can be used for accurate cluster extraction from large remote-sensing-images in an unsupervised manner. The ASCE2 can be helpful especially for agricultural monitoring (encompassing a whole country) where it is often hard and expensive to obtain labeled training samples for supervised classification methods.

The ASCE2 is based on data representative level ensemble approach, which in turn limits the ensemble on one kind of representative selection (neural gas in our study). However, the use of different quantization approaches (such as k-means, self-organising maps, or their variants) or different initializations may produce distinct partitionings, which are then to be fused by an ensemble approach. Yet, graph-based ensemble would be infeasible at the data level for large remote-sensing images due to its complexity, while maximum voting would be unsuccessful based on our preliminary studies. An ensemble approach tailored for ASC of large datasets would help for more effective partitionings. With its current settings using neural gas quantization, the proposed ASCE2 already achieves significant performances for the remote-sensing images in this study.

References

[1] L. A. Ruiz, A. Fdez-Sarria, and J. A. Recio, "Texture feature extraction for classification of remote sensing data using wavelet decomposition: A comparative study," in *Proc. Int. Arch. Photogramm. Remote Sens*., 2004, vol. 35, pp. 1682–1750.

[2] E. M. Wood, A. M. Pidgeon, V. C. Radeloff, and N. S. Keuler, "Image texture as a remotely sensed measure of vegetation structure," *Remote Sens. Environ.*, vol. 121, pp. 516–526, Jun. 2012.

[3] J. Yuan, D. Wang, and R. Li, "Remote sensing image segmentation by combining spectral and texture features," *IEEE Trans. Geosci. Remote Sens.*, vol. 52, no. 1, pp. 16–24, Jan. 2014.

[4] P. Mitra, U. Shankar, and S. Pal, "Segmentation of multispectral remote sensing images using active support vector machines," *Pattern Recognit. Lett.*, vol. 25, no. 9, pp. 1067–1074, Jul. 2004.

[5] R. Xu and D. Wunsch II, "Survey of clustering algorithms," *IEEE Trans. Neural Netw.*, vol. 16, no. 3, pp. 645–678, May 2005.

[6] K. Taşdemir, P. Milenov, and B. Tapsall, "A hybrid method combining SOM-based clustering and object-based analysis for identifying land in good agricultural condition," *Comput. Electron. Agric.*, vol. 83, pp. 92–101, 2012.

[7] M. L. Goncalves, M. L. A. Netto, J. A. F. Costa, and J. K. Zullo, "An unsupervised method of classifying remotely sensed images using Kohonen self-organizing maps and agglomerative hierarchical clustering methods," *Int. J. Remote Sens.*, vol. 29, no. 11, pp. 3171–3207, 2008.

[8] K. Taşdemir, P. Milenov, and B. Tapsall, "Topology-based hierarchical clustering of self-organizing maps," *IEEE Trans. Neural Netw.*, vol. 22, no. 3, pp. 474–485, Feb. 2011.

[9] T. Villmann, E. Merényi, and B. Hammer, "Neural maps in remote sensing image analysis," *Neural Networks*, vols. 3–4, no. 16, pp. 389–403, 2003.

[10] X. Zhang, L. Jiao, F. Liu, L. Bo, and M. Gong, "Spectral clustering ensemble applied to SAR image segmentation," *IEEE Trans. Geosci. Remote Sens.*, vol. 46, no. 7, pp. 2126–2136, Jul. 2008.

[11] K. Ersahin, I. G. Cumming, and R. K. Ward, "Segmentation and classification of polarimetric SAR data using spectral graph partitioning," *IEEE Trans. Geosci. Remote Sens.*, vol. 48, no. 1, pp. 164–174, Jan. 2010.

Authorized licensed use limited to: Abdullah GUl Univ (KAYSERI ABDULLAH GUL UNIVERSITESI). Downloaded on March 31,2023 at 06:40:09 UTC from IEEE Xplore. Restrictions apply.

[12] K. Taşdemir, "Vector quantization based approximate spectral clustering of large datasets," *Pattern Recognit.*, vol. 45, no. 8, pp. 3034–3044, 2012.
[13] K. Taşdemir, B. Yalcin, and I. Yildirim, "Approximate spectral clustering with utilized similarity information using geodesic based hybrid distance measures," *Pattern Recognit.*, vol. 48, no. 4, pp. 1459–1471, 2015.
[14] C. Fowlkes, S. Belongie, F. Chung, and J. Malik, "Spectral grouping using the Nyström method," *IEEE Trans. Pattern Anal. Mach. Intell.*, vol. 26, no. 2, pp. 214–225, Feb. 2004.
[15] L. Wang, C. Leckie, K. Ramamohanarao, and J. C. Bezdek, "Approximate spectral clustering." in *PAKDD*, vol. 5476, T. Theeramunkong, B. Kijsirikul, N. Cercone, and T. B. Ho, Eds. New York, NY, USA: Springer, 2009, pp. 134–146.
[16] L. Wang, C. Leckie, R. Kotagiri, and J. Bezdek, "Approximate pairwise clustering for large data sets via sampling plus extension," *Pattern Recognit.*, vol. 44, no. 2, pp. 222–235, 2011.
[17] K. Taşdemir, Y. Moazzen, and I. Yildirim, "Geodesic based similarities for approximate spectral clustering," in *Proc. 22nd Int. Conf. Pattern Recognit.*, Stockholm, Sweden, Aug. 2014, pp. 1360–1364.
[18] A. Strehl and J. Ghosh, "Cluster ensembles—A knowledge reuse framework for combining multiple partitions," *J. Mach. Learn. Res.*, vol. 3, no. 3, pp. 583–617, Mar. 2002.
[19] S. Dudoit and J. Fridlyand, "Bagging to improve the accuracy of a clustering procedure," *Bioinformatics*, vol. 19, no. 9, pp. 1090–1099, 2003.
[20] A. Topchy, A. K. Jain, and W. Punch, "A mixture model for clustering ensembles," in *Proc. SIAM Int. Conf. Data Min.*, 2004, pp. 379–390.
[21] A. L. N. Fred and A. K. Jain, "Combining multiple clusterings using evidence accumulation," *IEEE Trans. Pattern Anal. Mach. Intell.*, vol. 27, no. 6, pp. 835–850, Jul. 2005.
[22] F. Tung, A. Wong, and D. A. Clausi, "Enabling scalable spectral clustering for image segmentation," *Pattern Recognit.*, vol. 43, no. 12, pp. 4069–4076, 2010.
[23] J. Jia, X. Xiao, and B. Liu, "Similarity-based spectral clustering ensemble selection," in *Proc. 9th Int. Conf. Fuzzy Syst. Knowl. Discov. (FSKD)*, May 2012, pp. 1071–1074.
[24] X. Peng, L. Zhang, and Z. Yi, "Scalable sparse subspace clustering," in *Proc. IEEE Conf. Comput. Vis. Pattern Recognit. (CVPR)*, Jun. 2013, pp. 430–437.
[25] T. Martinetz and K. Schulten, "Topology representing networks," *Neural Netw.*, vol. 7, no. 3, pp. 507–522, 1994.
[26] A. Asuncion and D. Newman. (2007). *UCI Machine Learning Repository* [Online]. Available: http://www.ics.uci.edu/~mlearn/MLRepository.html
[27] G. A. Carpenter, S. Martens, and O. J. Ogas, "Self-organizing information fusion and hierarchical knowledge discovery: A new framework using ARTMAP neural networks," *Neural Netw.*, vol. 18, no. 3, pp. 287–295, 2005.
[28] J. Shi and J. Malik, "Normalized cuts and image segmentation," *IEEE Trans. Pattern Anal. Mach. Intell.*, vol. 22, no. 8, pp. 888–905, Aug. 2000.
[29] A. Ng, M. Jordan, and Y. Weiss, "On spectral clustering: analysis and an algorithm," in *Proc. Adv. Neural Inf. Process. Syst.*, 2002, vol. 14, pp. 849–856.
[30] M. Meila and J. Shi, "A random walks view of spectral segmentation," in *Proc. 8th Int. Workshop Artif. Intell. Statist. (AISTATS)*, 2001.
[31] U. von Luxburg, "A tutorial on spectral clustering," *J. Statist. Comput.*, vol. 17, no. 4, pp. 395–416, 2007.
[32] D. Verma and M. Meila, "A comparison of spectral clustering algorithms," Univ. Washington, Seattle, WA, USA, Tech. Rep. UW TR CSE-03-05-01, 2003.
[33] L. Zelnik-Manor and P. Perona, "Self-tuning spectral clustering," in *Proc. Adv. Neural Inf. Process. Syst.*, 2004.
[34] K. Taşdemir, "A hybrid similarity measure for approximate spectral clustering of remote sensing images," in *Proc. IEEE Int. Geosci. Remote Sens. Symp. (IGARSS)*, Jul. 2013, pp. 3136–3139.
[35] K. Taşdemir and E. Merényi, "Exploiting data topology in visualization and clustering of self-organizing maps," *IEEE Trans. Neural Netw.*, vol. 20, no. 4, pp. 549–562, Mar. 2009.
[36] L. Hubert and P. Arabie, "Comparing partitions," *J. Classification*, vol. 2, no. 1, pp. 193–218, 1985.
[37] C. D. Manning, P. Raghavan, and H. Schtze, *Introduction to Information Retrieval*. Cambridge, U.K.: Cambridge Univ. Press, 2008.
[38] S. Reis and K. Taşdemir, "Identification of hazelnut fields using spectral and gabor textural features," *ISPRS J. Photogramm. Remote Sens.*, vol. 66, no. 5, pp. 652–661, Sep. 2011.
[39] K. Taşdemir and S. Reis, "Land cover identification for finding hazelnut fields using worldview-2 imagery," in *Proc. IEEE Int. Geosci. Remote Sens. Symp. (IGARSS)*, 2011, pp. 158–161.
[40] J. Santos and M. Embrechts, "On the use of the adjusted rand index as a metric for evaluating supervised classification," in *Proc. Int. Conf. Artif. Neural Netw. (ICANN'09)*, Limassol, Cyprus, Sep. 2009, pp. 175–184.
[41] G. Wilkinson, "Results and implications of a study of fifteen years of satellite image classification experiments," *IEEE Trans. Geosci. Remote Sens.*, vol. 43, no. 3, pp. 433–440, Mar. 2005.
[42] C. Persello and L. Bruzzone, "Active and semi-supervised learning for the classification of remote sensing images," *IEEE Trans. Geosci. Remote Sens.*, vol. 52, no. 11, pp. 6937–6956, May 2014.

Kadim Taşdemir (M'09) received the B.S. degree in electrical and electronics engineering from Bogazici University, Istanbul, Turkey, the M.S. degree in computer engineering from Istanbul Technical University, Istanbul, Turkey, and the Ph.D. degree in electrical and computer engineering from Rice University, Houston, TX, USA, in 2001, 2004, and 2008, respectively.

Before joining AIU, he was a Researcher with the European Commission Joint Research Centre (JRC), Institute for Environment and Sustainability, Ispra, Italy, between 2009 and 2012, where he worked on automated control methods for monitoring agricultural resources using remote sensing imagery. He is a recipient of FP7 Marie Curie Career Integration Grant and TUBITAK Career Grant. His research interests include detailed knowledge discovery from high-dimensional and large data (especially remote sensing imagery) using machine learning (self-organized learning in particular), data mining, and pattern recognition.

Dr. Taşdemir is a member of IAPR-TC7 Remote Sensing and Mapping, and IAPR-TC15 Graph Based Representations. He is the Founding Chair of GRSS Turkey Chapter. He is a Reviewer for several journals including the IEEE TRANSACTIONS ON GEOSCIENCE AND REMOTE SENSING, the IEEE JOURNAL OF SELECTED TOPICS IN APPLIED EARTH OBSERVATIONS AND REMOTE SENSING, the IEEE TRANSACTIONS ON NEURAL NETWORKS AND LEARNING SYSTEMS, the IEEE TRANSACTIONS ON IMAGE PROCESSING, the IEEE TRANSACTIONS ON CYBERNETICS, *ISPRS Journal of Photogrammetry and Remote Sensing*, *International Journal of Remote Sensing*, and *Neural Processing Letters*. Based on his research excellence and contribution, he received 2011 IES Best Young Scientist Award. He was also awarded "Rice University Robert Patten Award" for his contributions to graduate life during his Ph.D.

Yaser Moazzen is currently pursuing the Graduate degree in biomedical engineering at the Department of Electronics and Communication Engineering, Istanbul Technical University, Istanbul, Turkey.

His research interests include pattern recognition and unsupervised clustering.

Isa Yildirim received the the B.Sc. degree in electronics and communication engineering and the M.Sc. degree in satellite communications and remote sensing program from Istanbul Technical University, Istanbul, Turkey, in 2002 and 2004, respectively, and the Ph.D. degree in electrical and computer engineering from the University of Illinois, Chicago, IL, USA, in 2009.

He is an Assistant Professor with the Department of Electronics and Communication Engineering, Istanbul Technical University. He is also an Adjunct Professor with Abdullah Gul University, Kayseri, Turkey, and University of Illinois, Chicago, IL, USA. His research interests include biomedical imaging, signal and image processing, compressed sensing, and pattern recognition. His research in biomedical imaging has been supported by NIH and TUBITAK.

Dr. Yildirim is an Associate Editor of the Turkish *Journal of Electrical Engineering and Computer Sciences* and is a Reviewer for several journals including the IEEE TRANSACTIONS ON BIOMEDICAL ENGINEERING, the IEEE TRANSACTIONS ON MEDICAL IMAGING, Springer *Multidimensional Systems and Signal Processing Journal*, Elsevier *Biomedical Signal Processing and Control Journal*, Elsevier *Computers in Medicine and Biology Journal*.

Authorized licensed use limited to: Abdullah GUl Univ (KAYSERI ABDULLAH GUL UNIVERSITESI). Downloaded on March 31,2023 at 06:40:09 UTC from IEEE Xplore. Restrictions apply.